Deb, A. K., "Theory of Sand Filtration," *Proc. ASCE, J. Sanitary Eng. Div.*, **95**, 399 (1969).
Herzig, J. P., D. M. Leclerc, and P. LeGoff, "Flow of Suspensions through Porous Media—Application to Deep Bed Filtration," *Ind. Eng. Chem.*, **62**, 8 (1970).
Hsiung, Kuo-ying, "Prediction of Performance of Granular Filters for Water Treatment," Ph.D. dissertation, Iowa State Univ., Ames (1967).
———, and J. L. Cleasby, "Prediction of Filter Performance," *Proc. ASCE, J. San. Eng. Div.*, **94**, No. SA4, 1043 (1968).
Huang, J. Y. C., and E. R. Bauman, "Least Cost Sand Filter for Iron Removal," *ibid.*, **97**, No. SA2, 171 (1971).
Hutchinson, H.P., and D. N. Sutherland, "An Open-Structure Open Solid," *Nature*, **206**, 1063 (1965).
Ives, K. J., "Rational Design of Filters," *Proc. Inst. Civil Engrs. (London)*, **16**, 189 (1960).
———, "Filtration Using Reduction Algae," *Proc. ASCE, J. Sanitary Eng. Div.*, **87**, No. SA3, 23 (1961).
———, "Simplified Rational Analysis of Filter Behavior," *Proc. Inst. Civil Engrs. (London)*, **25**, 345 (1963).
———, "Theory of Filtration," Special Lecture, No. 7 Int'l Water Supply Congress and Exhibition, Vienna (1969).
Maraudas, A., Ph.D. dissertation, London Univ., England (1961).
———, and P. Eisenklam, "Clarification of Suspensions: A Study of Particle Deposition in Granular Media. Part I—Some Observations on Particle Deposition," *Chem. Eng. Sci.*, **20**, 867 (1965).
———, "Part II—A Theory of Clarification," *ibid.*, 875 (1965).
Mohanka, S. S., "Theory of Multistage Filtration," *Proc. ASCE, J. Sanitary Eng. Div.*, **95**, SA6, 1079 (1969).
Payatakes, A. C., Chi Tien, and R. M. Turian, "A New Model for Granular Porous Media—Part I Model Formulation," *AIChE J.*, **19**, 58 (1973*a*).
———, "A New Model for Granular Porous Media—Part II Numerical Solution of Steady State Incompressible Newtonian Flow Through Periodically Constricted Tubes," *ibid.*, 67 (1973*b*).
Pendse, H., Chi Tien, and R. M. Turian, "Dispersion Measurement in Clogged Filter Beds—A Diagnostic Study on the Morphology of Particle Deposits," *AIChE J.*, **24**, 473 (1978).
Rajagopalan, R., and Chi Tien, "Trajectory Analysis of Deep Bed Filtration Using the Sphere-in-cell Porous Media Model," *AIChE J.*, **22**, 523 (1976).
———, "Single Collector Analysis of Collection Mechanisms in Water Filtration," *Can. J. Chem. Eng.*, **55**, 246 (1977).
Rimer, A. E., "Filtration Through a Trimedia Filter," *Proc. ASCE, J. Sanitary Eng. Div.*, **94**, SA No. 3, 521 (1968).
Spielman, L. A., and J. A. FitzPatrick, "Deposition of Non-Brownian Particles Under Colloidal Forces," *J. Colloid Interface Sci.*, **43**, 51 (1973).
Wnek, W. J., D. Gidaspow, and D. T. Wasan, "The Role of Colloidal Chemistry in Modelling Deep Bed Liquid Filtration," *Chem. Eng. Sci.*, **30**, 1035 (1975).
Yao, K.-M., M. T. Habibian, and C. R. O'Melia, "Water and Waste Water Filtration Concepts and Applications," *Environ. Sci. Technol.*, **5**, 1105 (1971).

Manuscript received February 20, 1978; revision received November 20, and accepted January 3, 1979.

A Gas Convection Model of Heat Transfer in Large Particle Fluidized Beds

A steady gas convection model of heat transfer to a horizontal cylinder immersed in a large particle gas fluidized bed has been developed. The model is based upon the hypothesis that the large particles will be isothermal and includes the effect of radiation as well as interstitial turbulence.

Results of calculations based on the model, for a two-dimensional bubbling bed, indicate that a single bubble, having a diameter equal to the cylinder diameter, has a relatively small influence on the total heat transfer.

RONALD L. ADAMS
and
JAMES R. WELTY
Department of Mechanical Engineering
Oregon State University
Corvallis, Oregon 97331

SCOPE

Fluidized bed combustion is currently being studied intensively since beds containing limestone or dolomite will adsorb sulfur dioxide, thereby providing a way to burn high sulfur coals to generate power while maintaining air quality standards. The atmospheric pressure fluid bed combustor is expected to operate at a temperature of about 1 100°K and contain particles with mean diameters as large as 6 mm. Current heat exchanger designs are based on horizontal tube arrangements, so heat transfer to horizontal cylinders either singly or in banks immersed in a large particle bed is of interest.

Heat transfer to surfaces immersed in a large particle fluidized bed such as the atmospheric combustor is expected to occur principally by gas convection. Accordingly, a gas convection heat transfer model has been developed considering the flow within interstitial voids adjacent to the surface as well as within bubbles contacting the surface. Radiation heat transfer from the hot particles, important at combustion temperatures, is also included, and the effect of interstitial turbulence is incorporated in the convection model. Most previous models of fluid bed heat transfer were developed for beds containing small particles in which unsteady conduction is the dominant mode of heat transfer and are considered inadequate for the analysis of heat transfer to a horizontal cylinder immersed in a large particle bed in which gas convection is the dominant mode of heat transfer.

Ronald L. Adams is with Massachusetts Institute of Technology Lincoln Laboratory, P.O. Box 73, Lexington, Mass. 02173.

The convective heat transfer due to flow in the interstitial voids is obtained from analysis of flow within channels between particles contacting the cylinder wall. This channel flow is analyzed by considering separately a region of three-dimensional boundary-layer flow near the particle contact points and a two-dimensional boundary-layer flow halfway between contact points. This channel flow model is used for both the windward side of the cylinder, where particles are expected to be loosely packed, as well as the more densely packed stack on the leeward side (lee stack). The convective heat transfer due to flow within a contacting bubble is obtained from a two-dimensional boundary-layer analysis.

CONCLUSIONS AND SIGNIFICANCE

Results were obtained for heat transfer to a horizontal cylinder immersed in a two-dimensional bubbling bed operating at atmospheric pressure with both cold (300°K) and hot (1 100°K) flow. The effect of a single bubble, having a diameter equal to the cylinder diameter, on both the total heat transfer to the cylinder and the distribution on the cylinder surface has been obtained for 3 and 6 mm mean diameter limestone particles. The effect of the bubble on the total heat transfer was found to be relatively small (a decrease of at most 27% for bubble center positions close to the cylinder wall), but the heat transfer distributions are strongly affected when the bubble is contacting the cylinder (some local values change by a factor of 3 or more). Interstitial turbulence was found to have a lesser effect at high temperatures than at low temperatures for a given particle size. Approximately 33% of the heat transfer occurred by radiation for the hot flow cases.

The assumptions of the model are expected to be valid for particle diameters greater than 2 to 3 mm. Detailed experimental work is required to completely validate the model, though the total heat transfer coefficients calculated are within the range of experimental data obtained by Wright et al. (1970).

Fluidized bed combustion is currently being studied intensively because beds containing limestone or dolomite will adsorb sulfur dioxide, thereby providing a way to burn high sulfur coals to generate power while maintaining air quality standards. The design of a fluid bed combustor is dependent upon internal heat transfer rates, and current interest is in designs based upon horizontal arrangements of standard heat exchanger tubes (typically 0.05 m diameter). The operating parameters for the atmospheric pressure fluid bed combustor result in consideration of limestone particle diameters as large as 6 mm, with combustion temperatures around 1 100°K. Accordingly, heat transfer rates to a horizontal cylinder immersed in a high temperature fluidized bed containing large particles are required for boiler design.

The packing in the vicinity of a horizontal cylinder immersed in a gas fluidized bed is typically as shown in Figure 1. Generally, large gas voids or bubbles sweep

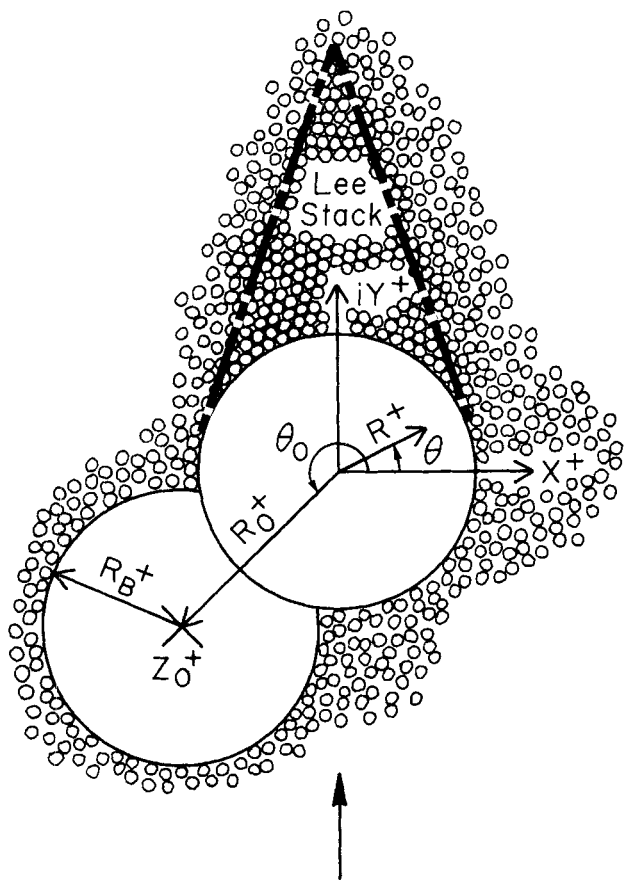

Fig. 1. Packing near a horizontal cylinder.

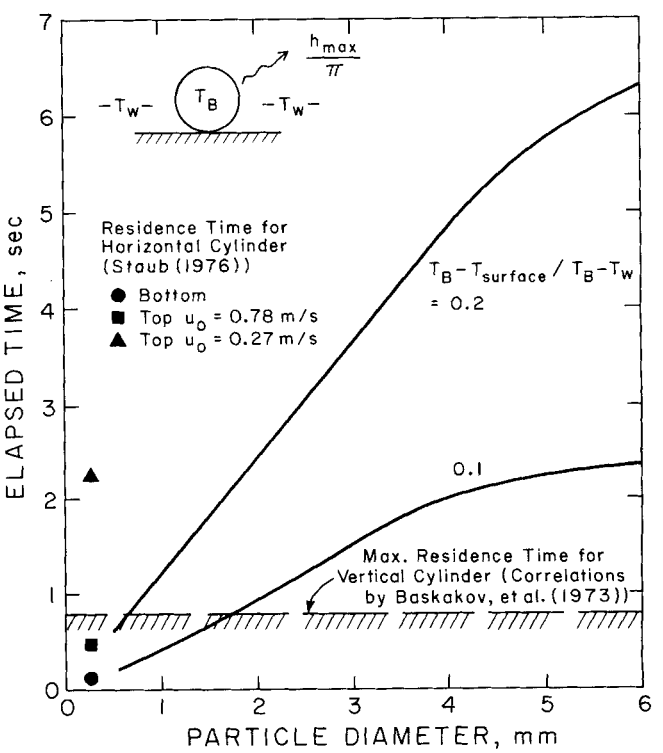

Fig. 2. Transient cooling of a spherical limestone particle.

by the cylinder pushing particles away from the surface as shown. Also, a relatively stagnant, closely packed stack of particles forms on the leeward side of the cylinder (lee stack), while particles on the windward side are more loosely packed and more dynamic. The particles on the windward side are in nearly continuous motion, while the lee stack is only periodically removed and replenished as bubbles pass the cylinder.

Large particles tend to remain isothermal during their residence time near a surface immersed in a fluid bed. This isothermal behavior is demonstrated for limestone particles in Figure 2 which compares residence time with the time required to convectively reduce the relative surface temperature by 10 and 20% as a function of particle size. This estimate was obtained by assuming that cooling occurs by convection to a bath at the wall temperature and with a heat transfer coefficient equal to the maximum fluid bed values for the given particle sizes (adjusted for surface area). Shown for comparison are typical particle residence times at surfaces of horizontal and vertical cylinders.

In a fluidized bed containing large particles and operating at moderate values of u_0/u_{mf}, the interstitial gas velocity is much larger than both bubble velocities and particle velocities induced by bubble motion. This results from the independence of bubble velocity and fluidizing velocity in beds with superficial velocities near u_{mf}. As a result of this slow bubble condition, unsteady effects on the gas flow due to bubble and particle motions will be small, and the interstitial gas velocity will be determined by the instantaneous packing conditions in the vicinity of the surface.

Since the particles are expected to be isothermal, and unsteady effects are expected to be small at moderate superficial velocities in large particle beds, heat transfer to an immersed surface is primarily due to the steady flow of gas within the interstitial voids formed by the isothermal particles and the cylinder wall and within bubbles contacting the wall. This convective heat transfer will be amplified by the turbulence generated in the wakes of the solid particles. Thermal radiation will also contribute to the heat transfer, but the effect of emission and absorption in the gas is small. In fact, for the atmospheric pressure combustor, the gas will be optically thin over approximately three cylinder diameters (for 0.05 m diameter cylinder), and the nondimensional gas energy equation reveals that the ratio of emission to convection is about $1/Re_D$. Thus radiation heat transfer will occur by direct emission from the hot particle surfaces. Furthermore, Basu (1978) has shown that the effect of combustion on heat transfer is insignificant for coal content less than 10%, and so it will be neglected.

Many analytical models have been developed for heat transfer to surfaces immersed in small particle fluidized beds in which unsteady conduction from the particles is the dominant mode of heat transfer (see, for example, Botterill, 1975). Most of these models are based upon consideration of a packet of material (solid particles and gas) which is swept up to the heat transfer surface and exchanges energy by unsteady conduction. Differences in the various models are primarily differences in modeling the characteristics of the packet. This packet was treated as a continuum by Mickley and Fairbanks (1955), and their model was refined and modified by a number of investigators; for example, Yoshida et al. (1969), Wasan and Ahluwalia (1969), Chung et al. (1972), Broughton and Kubie (1975), and others. A model based upon discrete particles dispersed throughout the gas was developed by Botterill and Williams (1963). Ziegler et al. (1964) also used a discrete particle model but assumed that the gas phase is at the wall temperature and heat is transferred from the particles by convection to the gas phase. Basu (1978) used this same discrete particle model in his analysis of the effect of combustion on heat transfer, and Gabor (1972) based his model on unsteady conduction in alternate states of solid and gas. A key parameter in all of these models is the residence time distribution of the packet, and the continuum approaches require thermal properties of the packet as well.

Very little analytical work has been directed toward heat transfer in large particle beds in which gas convection is the dominant mode, though a few gas convection based models have been developed. One of the first of these was based upon scouring of the gas boundary layer at particle contact points (a two-dimensional view of the interstitial boundary-layer development) and was developed by Levenspiel and Walton (1954). Also, Baskakov et al. (1973) have developed an empirical model for this regime based upon experimental data obtained by Baskakov and Suprum (1972). Recently, Botterill and Denloye (1978) extended a packed-bed model, based upon one-dimensional flow and an effective conductivity, to estimate heat transfer to a vertical cylinder due to gas convection. None of these models adequately treats heat transfer due to the three-dimensional interstitial flow in the presence of isothermal, hot particles and due to flow within bubbles contacting the immersed surface.

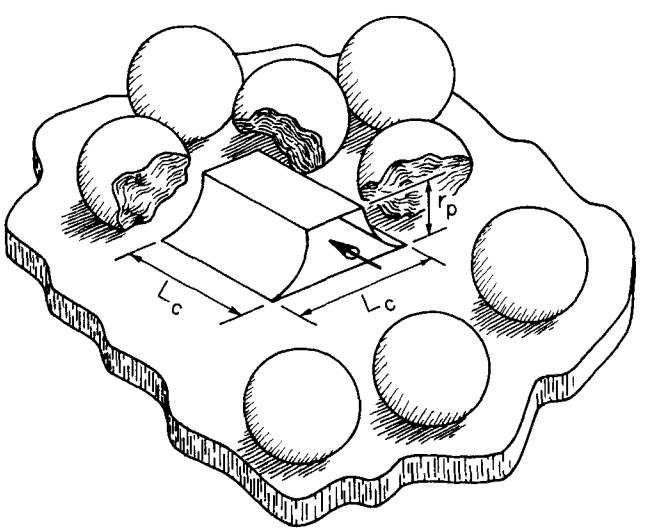

Fig. 3. Interstitial channel.

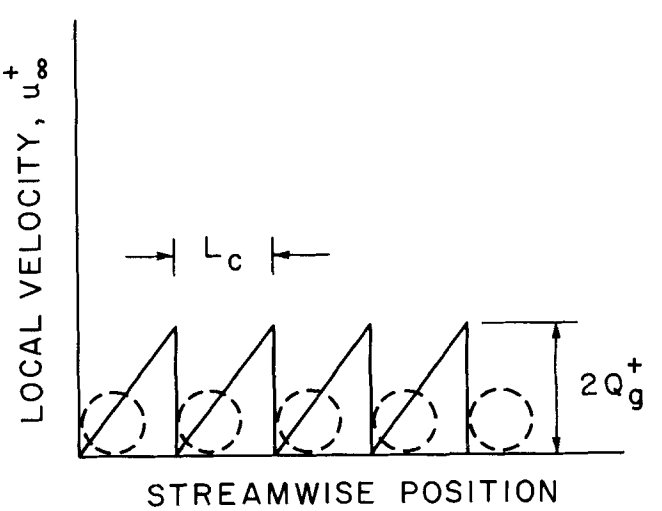

Fig. 4. Assumed variation of local interstitial velocity.

INTERSTITIAL CHANNEL MODEL

The convective heat transfer due to flow in the interstitial voids adjacent to the cylinder wall is modeled by considering flow within the channel shown in Figure 3. This flow channel is bounded below by the cylinder wall and on the sides by surfaces approximately defining the circulating gas trapped between adjacent particles. The geometry of the channel is further specified by requiring the length and width at the base to be equal to the average spacing between particles. This spacing is determined from the local voidage at the surface of the cylinder.

The thickness of the gas boundary layer which forms along the lower surface of the channel (cylinder wall) is expected to be much smaller than the height of the channel, so gas flow in the central core of the channel is assumed to be inviscid. Furthermore, the gas is assumed to be at bed temperature in the core. The core velocity variation is estimated through consideration of the nature of the interstitial flow in general. This flow has been described by Galloway and Sage (1970) as a series of jets, wakes, and stagnant regions with rapid changes in velocity near particle surfaces. Detailed analytical determination of this flow is nearly impossible, so a simple model is used in which the core velocity is assumed to vanish when a solid particle is encountered, then increase linearly over the length of the channel until another particle is encountered as shown in Figure 4. The actual magnitude of the velocity at the end of the channel is established from analytical determination of the average interstitial velocity. This assumed velocity variation will result in a thinning of the boundary layer due to acceleration, consistent with the expected physical behavior of the three-dimensional flow.

The gas flow in the boundary-layer portion of the interstitial channel will be three-dimensional owing to the cusped corner between the upper surface and the cylinder wall, and this will produce a three-dimensional temperature field as well. However, the flow in these corner regions is assumed to be Stokeslike so that the convective terms in the momentum and energy equations are neglected, while the boundary layer in the central region of the channel away from the corners is assumed to be two-dimensional.

ANALYSIS

The convective heat transfer due to flow in the two-dimensional portion of the interstitial channels and within a contacting bubble is obtained from an integral solution of the two-dimensional boundary-layer equations. The effect of interstitial turbulence on the solution is much like the effect of free stream turbulence on the heat transfer to objects immersed in an air stream for which similarity solutions have been obtained, for example, Smith and Kuethe (1966) and Traci and Wilcox (1975). The effect is included here in an integral solution by introducing a transformation which effectively stretches the normal coordinate. Since gas property variations have a small effect on heat transfer (see Levy, 1954, or Kays, 1966), the constant property form of the low speed boundary-layer equations will be used, and the effect of turbulence will be included through an eddy diffusivity term in the time averaged equations. In dimensionless form, they are

$$\frac{\partial v^+}{\partial y^+} + \frac{\partial u^+}{\partial z^+} = 0 \tag{1}$$

$$v^+ \frac{\partial u^+}{\partial y^+} + u^+ \frac{\partial u^+}{\partial z^+} = -\frac{dp^+}{dz^+} + \frac{1}{Re_D} \frac{\partial}{\partial y^+}\left[(1 + \epsilon_T{}^+) \frac{\partial u^+}{\partial y^+} \right] \tag{2}$$

$$v^+ \frac{\partial \theta^+}{\partial y^+} + u^+ \frac{\partial \theta^+}{\partial z^+} = \frac{1}{Re_D Pr} \frac{\partial}{\partial y^+}\left[(1 + \epsilon_T{}^+) \frac{\partial \theta^+}{\partial y^+} \right] \tag{3}$$

where $\epsilon_T{}^+$ is the dimensionless eddy diffusivity, and eddy diffusivities of heat and momentum are assumed to be equal and isotropic. Also, the boundary conditions are

at $y^+ = 0$ (cylinder wall)

$$u^+ = 0 \tag{4a}$$

$$v^+ = 0 \tag{4b}$$

$$\theta^+ = 0 \tag{4c}$$

$$\epsilon_T{}^+ = 0 \tag{4d}$$

Thus

$$\frac{\partial}{\partial y^+}\left[(1 + \epsilon_T{}^+) \frac{\partial u^+}{\partial y^+} \right] = \frac{dp^+}{dz^+} \tag{4e}$$

and

$$\frac{\partial}{\partial y^+}\left[(1 + \epsilon_T{}^+) \frac{\partial \theta^+}{\partial y^+} \right] = 0 \tag{4f}$$

At $y^+ = \delta$ (edge of boundary layer)

$$u^+ = u_\infty{}^+ \tag{5a}$$

$$\theta^+ = 1 \tag{5b}$$

$$\frac{\partial u^+}{\partial y^+} = 0 = \frac{\partial^2 u^+}{\partial y^{+2}} \tag{5c}$$

$$\frac{\partial \theta^+}{\partial y^+} = 0 = \frac{\partial^2 \theta^+}{\partial y^{+2}} \tag{5d}$$

$$\epsilon_T{}^+ = \epsilon_{T\infty}/\nu_\infty = \beta_T \tag{5e}$$

The integral transformation $d\xi = dy^+/1 + \epsilon_T{}^+$ is introduced to absorb the interstitial turbulence in the normal coordinate, and Equations (1) to (3) are integrated across the boundary layer following the von-Kármán-Pohlhausen approach (see Schlichting, 1968) to obtain

$$\frac{d}{dz^+}\left\{ \int_0^{\delta_V} u^+ (u_\infty{}^+ - u^+)(1 + \epsilon_T{}^+) d\xi \right\} + \left\{ \int_0^{\delta_V} (u_\infty{}^+ - u^+)(1 + \epsilon_T{}^+) d\xi \right\} \frac{du_\infty{}^+}{dz^+} = \frac{1}{Re_D} \frac{\partial u^+}{\partial \xi}(0) \tag{6}$$

$$\frac{d}{dz^+}\left\{ \int_0^{\delta_H} u^+ (1 - \theta^+)(1 + \epsilon_T{}^+) d\xi \right\} = \frac{1}{Re_D Pr} \frac{\partial \theta^+}{\partial \xi}(0) \tag{7}$$

These equations are further reduced to

$$\frac{d}{dz^+}(M u_\infty{}^+) = 2\left[\frac{H_{2V}}{u_\infty{}^+} \frac{\partial u^+}{\partial \xi}(0) - \left(\frac{3}{2} + H_{12} \right) M \frac{du_\infty{}^+}{dz^+} \right] \tag{8}$$

$$\frac{d}{dz^+}(W u_\infty{}^+) = 2G_{2H} \frac{\partial \theta^+}{\partial \xi}(0) - W \frac{du_\infty{}^+}{dz^+} \tag{9}$$

where $M = Re_D \delta_2{}^2$, $W = Re_D Pr\, \Delta_2{}^2$, and

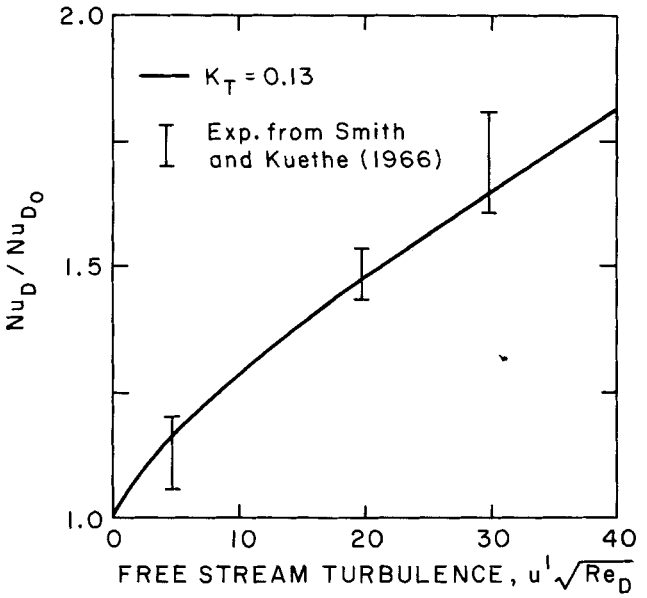

Fig. 5. Effect of free stream turbulence on stagnation point heat transfer for a cylinder.

$$\delta_1 = \int_0^{\delta_V} \left(1 - \frac{u^+}{u_\infty^+}\right)(1 + \epsilon_T^+)\,d\xi \qquad (10)$$

$$\delta_2 = \int_0^{\delta_V} \frac{u^+}{u_\infty^+}\left(1 - \frac{u^+}{u_\infty^+}\right)(1 + \epsilon_T^+)\,d\xi \qquad (11)$$

$$\Delta_2 = \int_0^{\delta_H} \frac{u^+}{u_\infty^+}(1 - \theta^+)(1 + \epsilon_T^+)\,d\xi \qquad (12)$$

$$H_{2V} = \frac{\delta_2}{\delta_V} \qquad (13)$$

$$H_{12} = \frac{\delta_1}{\delta_2} \qquad (14)$$

$$G_{2H} = \frac{\Delta_2}{\delta_H} \qquad (15)$$

Appropriate profiles for u^+, θ^+, and ϵ_T^+ must now be introduced and fitted to the boundary conditions so that the integral parameters can be evaluated. Following Pohlhausen's analysis, we assume the following profiles:

$$\frac{u^+}{u_\infty^+} = a_1\eta_V + a_2\eta_V^2 + a_3\eta_V^3 + a_4\eta_V^4 \qquad (16)$$

$$\theta^+ = b_1\eta_H + b_2\eta_H^2 + b_3\eta_H^3 + b_4\eta_H^4 \qquad (17)$$

where

$$\eta_V = \xi/\delta_V \quad \text{and} \quad \eta_H = \xi/\delta_H$$

and the eddy diffusivity is assumed to be linear in η_V. The boundary conditions [Equations (4) and (5)] are used to establish the profile parameters. Then, evaluation of the integrals reveals the true dependent variables to be the velocity profile shape parameter $\Omega_V = Re_D\,\delta_V^2\,\dfrac{du_\infty^+}{dz^+}$ and the thickness ratio $N_{HV} = \delta_H/\delta_V$. Numerical solution of Equations (8) and (9) provides Ω_V and N_{HV} as a function of the turbulence parameter β_T. Then, the Nusselt number is

$$Nu_D = \frac{\partial\theta^+}{\partial y^+} = \frac{2}{\delta_H} = \frac{2}{N_{HV}\left[\dfrac{\Omega_V}{Re_D\dfrac{du^+}{dz^+}}\right]^{1/2}} \qquad (18)$$

The turbulence parameter β_T is related to the interstitial turbulence intensity through

$$\beta_T = K_T\frac{u'u_\infty l_\infty}{\nu_\infty} \qquad (19)$$

where K_T is assumed to be a universal constant, and l_∞ is the length scale for the turbulence. Following Traci and Wilcox (1975), the turbulence length scale is assumed to be

$$l_\infty \sim \frac{L}{\sqrt{Re_{L_\infty}}} \qquad (20)$$

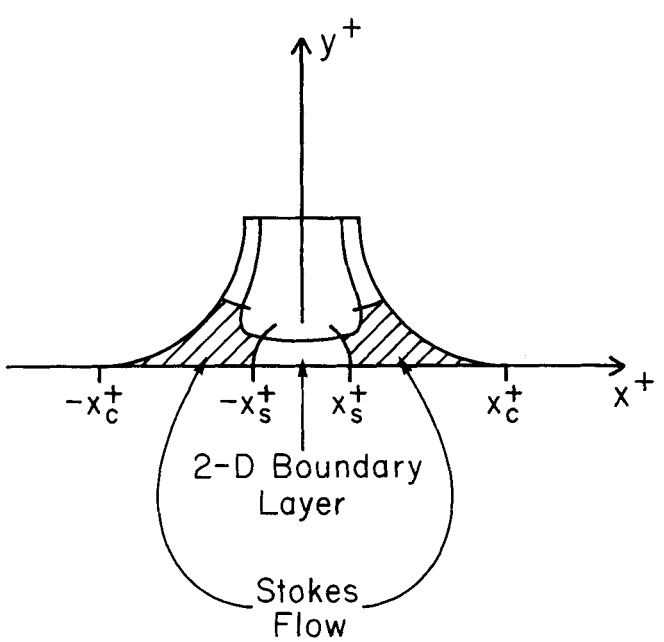

A. Physical Plane

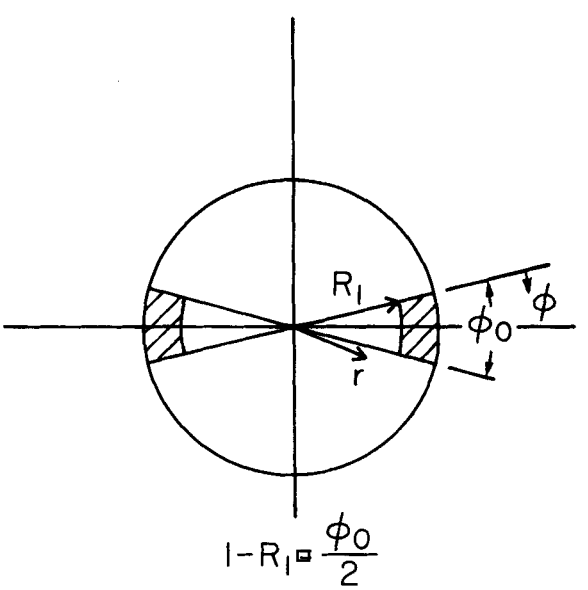

B. Circle Plane

Fig. 6. Stokes flow regions.

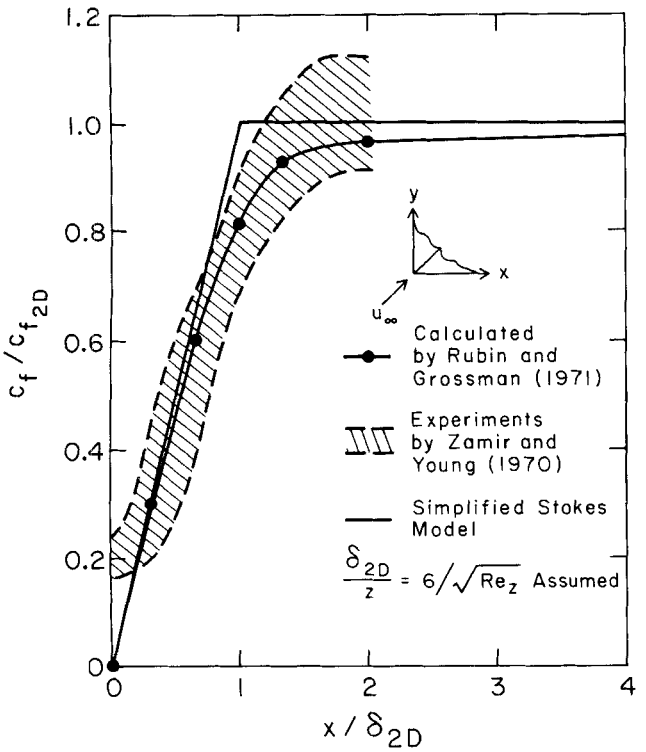

Fig. 7. Skin friction coefficient for flow along a right angle corner.

where L is an appropriate characteristic length (D for a cylinder in an air stream and d_p for a fluidized bed). Thus

$$\beta_T = K_T\, u' \sqrt{Re_{L_\infty}} \tag{21}$$

The universal constant K_T is obtained by matching predictions for stagnation point heat transfer for a cylinder in an air stream with experimental results. As shown in Figure 5, calculations performed using the integral analysis with $K_T = 0.13$ provide results which agree well with experimental data.

The Stokes flow assumption for the cusped interstitial corners reduces the analysis of heat transfer in these regions to solution of the steady conduction equation for the region shown in Figure 6*a*. The edge of this region along the cylinder wall is established by requiring

$$(Nu_D)_{\substack{\text{Stokes}\\ \text{edge}}} = (Nu_D)_{2D} \tag{22}$$

with $(Nu_D)_{2D}$ obtained from the two-dimensional boundary-layer analysis described above. The remaining boundaries of the region are assumed to be natural coordinates produced by the conformal mapping of a unit circle onto the channel cross section as shown in Figure 6*b*. Furthermore, the region is assumed to form a curvilinear rectangle on the unit circle with a width in the radial direction equal to half the length in the angular direction. These assumptions are based upon experimental results for the development of the boundary layer along a right angle corner obtained by Zamir and Young (1970). The validity of these assumptions and the two-region analysis described here is demonstrated for flow along a right angle corner in Figure 7. This figure provides a comparison of the two-region model with finite-difference calculations by Rubin and Grossman (1971) and experiments by Zamir and Young (1970) for the skin friction coefficient.

Utilizing Kirchoff's transformation (Arpaci, 1966) for thermal conductivity varying linearly with temperature and neglecting turbulence, the energy equation for the Stokes region is

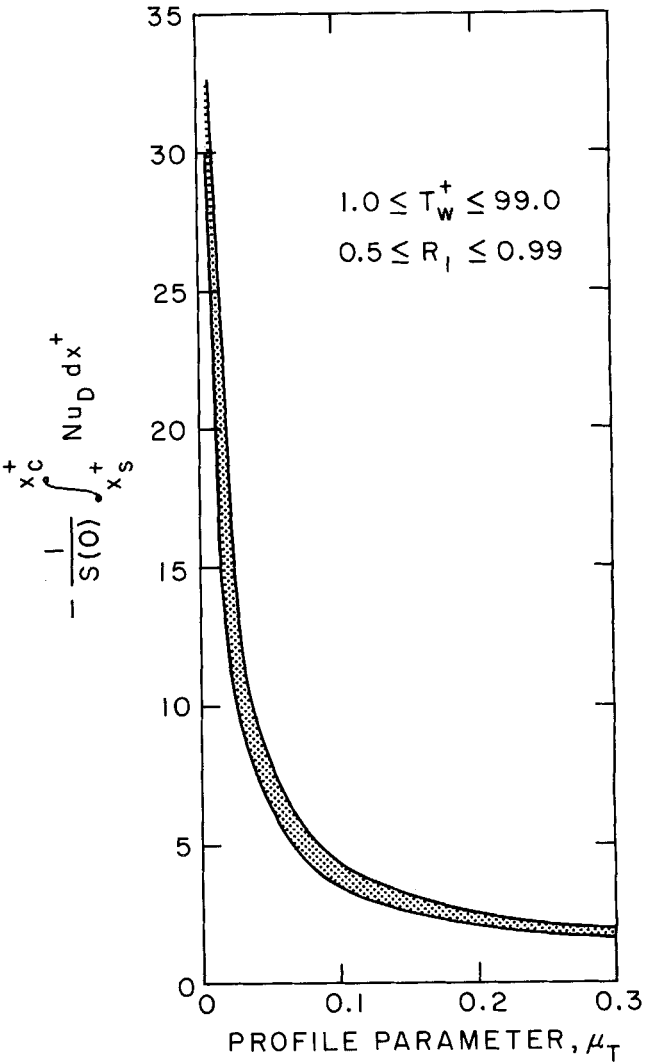

Fig. 8. Stokes region total energy parameter.

$$\nabla^2 S = 0 \tag{23}$$

where

$$S(\theta^+) = \frac{S(0)}{(0.5 + T_W^+)} \left[\frac{1}{2} (1 - \theta^{+2}) + T_W^+ (1 - \theta^+) \right] \tag{24}$$

Also, the boundary conditions on the circle plane are

$$\theta^+(1, \phi) = \left(1 - \frac{2\phi}{\phi_0}\right)^{\mu_T} \qquad 0 \le \phi \le \frac{\phi_0}{2} \tag{25a}$$

$$\theta^+(1, \phi) = 0 \qquad \frac{\phi_0}{2} < \phi \le \phi_0 \tag{25b}$$

$$\theta^+(R_1, \phi) = 1 \tag{25c}$$

$$\frac{\partial \theta^+}{\partial r}(r, 0) = \frac{\partial \theta^+}{\partial r}(r, \phi_0) = 0$$

where the parameter μ_T is determined so that the temperature variation along the curved portion of the physical boundary is approximately linear. The parameter μ_T can be approximated from the general relation for a straight sided corner mapping as

$$\mu_T \simeq \frac{\ln(x_c^+ - x^+)}{\ln(\phi - \phi_c)} \tag{26}$$

with $x^+(\phi)$ determined from the mapping function.

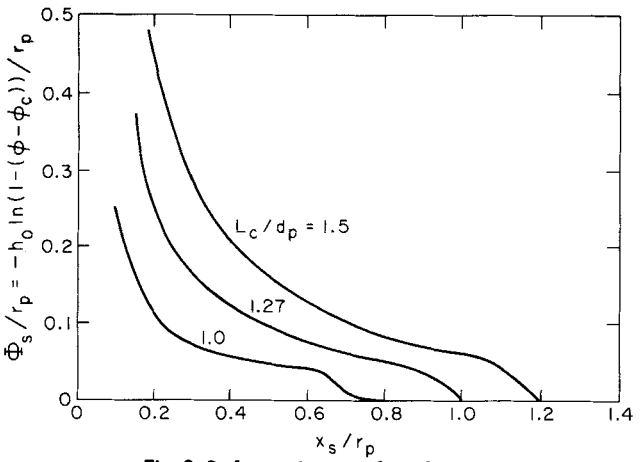

Fig. 9. Stokes region matching function.

Equation (23) is solved using separation of variables and the Fourier coefficients are obtained from the first two boundary conditions. The resulting expressions for the coefficients contain confluent hypergeometric functions, and analytic expressions for these are obtained by using the asymptotic forms (see Adams, 1977). The solution obtained in this manner is used to obtain the Nusselt number at the edge of the Stokes region (the matching parameter) and the total energy conducted to the wall. Results of computations over a broad range of the parameters R_1, $T_W{}^+$, and μ_T provided the approximation

$$(Nu_D)_{\substack{\text{Stokes}\\ \text{edge}}} \simeq -\frac{1.4\,S_0}{\Phi_s} \tag{27}$$

where $\Phi_s = -h_0 \ln[1-(\phi-\phi_c)]$ and is determined as a function of x^+ from the conformal mapping. Also, the variation in total energy is as shown in Figure 8.

The mapping function, required for determination of the parameter Φ_s, is obtained numerically using Theodoren's method (1933). Values of Φ_s for three particle spacings are shown in Figure 9, and μ_T was found to be 0.11 to 0.15 for particle spacings of 1 to 1.5 diam. Detailed derivations and the computation scheme can be found in Adams (1977).

The radiation heat transfer due to emission from the hot particle surfaces is obtained using the net radiation method (Siegel and Howell, 1972) and assuming that the particle strings adjacent to the cylinder wall and at the bubble boundary form isothermal gray surfaces as shown in Figure 10. The net radiation heat transfer is converted to effective Nusselt numbers to obtain

$$Nu^R_{D_1} = Bi^R \frac{e_p(T_B{}^{+4} - T_W{}^{+4})}{1 + e_p\left(\frac{1}{e_W} - 1\right)} \tag{28}$$

$$Nu^R_{D_2} = Bi^R \frac{e_B(T_B{}^{+4} - T_W{}^{+4})}{\frac{A_2}{A_3} + e_B\left(\frac{1}{e_W} - \frac{A_2}{A_3}\right)} \tag{29}$$

where $Bi^R = \dfrac{\sigma D}{K_g}(T_B - T_W)^3$ and the emissivity of the surface formed by the particles adjacent to the wall e_p is adjusted for cooling using the results of Baskakov et al. (1973).

Closure of the analysis described above is obtained when the average gas velocity at the cylinder wall is specified. This velocity can be obtained analytically for the case of a two-dimensional bubbling bed by using complex analysis. Since the interstitial velocity is large

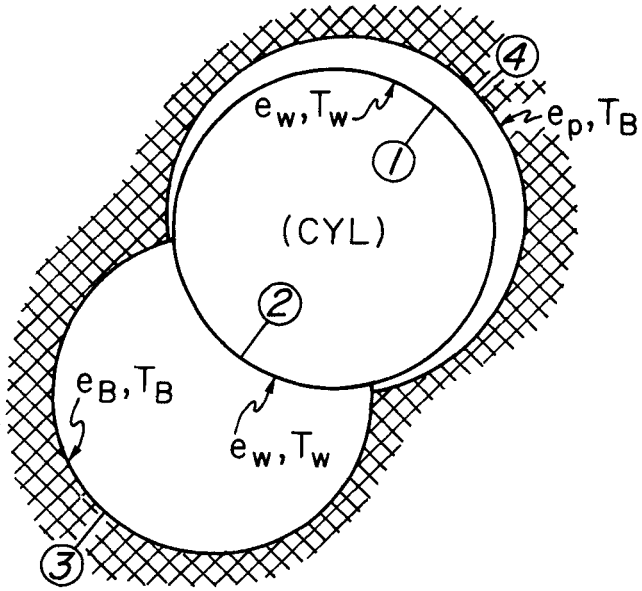

Fig. 10. Enclosures for radiative exchange calculation.

relative to the particle and bubble velocities, unsteady effects will be small, and the mean flow momentum equation valid outside the bubbles reduces to

$$\nabla p^+ = -K_\beta \overline{Q}_g{}^+ \tag{30}$$

K_β, the dimensionless drag coefficient, is obtained from pressure drop correlations for fixed beds (see Kunii and Levenspiel, 1962) and takes on the form

$$K_\beta = \frac{1}{d_p{}^+}\left(\frac{\beta_1}{Re_p} + \beta_2\right) \tag{31}$$

with

$$\beta_1 = 150\left(\frac{(1-\epsilon)}{\epsilon\phi_s}\right)^2 \tag{32}$$

$$\beta_2 = \frac{1.75}{\epsilon_\infty}\,\frac{1-\epsilon}{\epsilon\phi_s} \tag{33}$$

Variations in voidage are neglected in the determination of the pressure but are included later when the velocity is calculated. With these assumptions, the pressure field satisfies

$$\nabla^2 p^+ = 0 \tag{34}$$

with boundary conditions

$$\nabla p^+ = \left(\frac{dp^+}{dy^+}\right)_\infty \quad \text{far from the cylinder} \tag{35a}$$

$$\frac{\partial p}{\partial R} = 0 \quad \text{at the cylinder surface} \tag{35b}$$

Equation (34) is solved by the method of images (Batchelor, 1967), with the bubbles represented as doublets. The solution is

$$p^+ = \text{Real}\left\{-i\left(\frac{dp^+}{dy^+}\right)_\infty \left[z^+ - \frac{1}{4z^+} + \sum_{j=1}^{N} R_{Bj}{}^{+2}\left[\frac{1}{z^+ - z_{0j}{}^+} - \frac{1}{\frac{1}{4z^+} - \overline{z}_{0j}{}^+}\right]\right]\right\} \tag{36}$$

and the average interstitial velocity at the cylinder surface is

$$Q^+_{g\theta} = \frac{\frac{1}{2}\left(\frac{dp^+}{dy^+}\right)_x}{K_\beta}\left\{2\cos\theta + \sum_{j=1}^{N} R^*_{Bj}\left[\frac{-2\cos\theta - 4R^*_{0j}\sin(\theta-\theta_{0j})(R^*_{0j}\sin\theta_0 - \sin\theta)}{1+R^{*2}_{0j}-2R^*_{0j}\cos(\theta-\theta_{0j})[1+R^{*2}_{0j}-2R^*_{0j}\cos(\theta-\theta_{0j})]^2}\right]\right\} \quad (37)$$

The pressure solution is also used to obtain the average gas velocity within bubbles contacting the cylinder wall numerically by using conservation of mass. The average velocity distribution obtained for a bubble located as indicated and with lee stack and windward side voidages of 0.438 and 0.65, respectively, and with ambient voidage of 0.5 is shown in Figure 11.

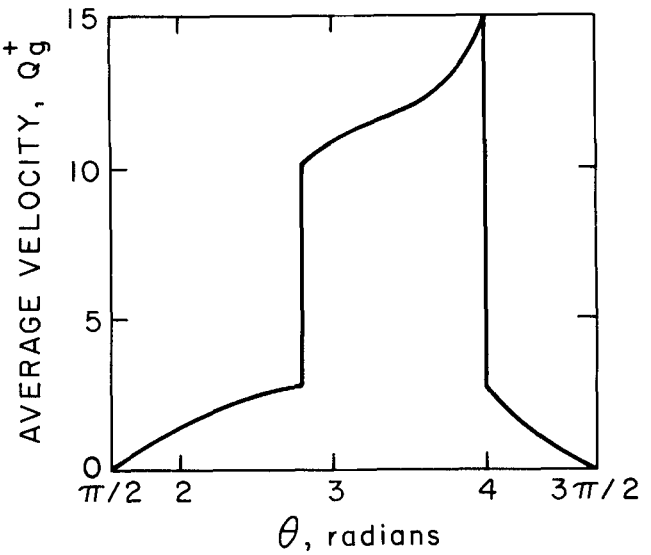

Fig. 11. Average velocity distribution with bubble at R^*, θ = 1.5, 3π/2, and $R_B{}^*$ = 1.

RESULTS

The analysis described above has been used to develop computer programs so that Nusselt number distributions on the cylinder surface as well as total heat transfer coefficients can be obtained. Computations were performed for limestone with mean particle diameters of 3 and 6 mm and bed temperatures of 1 117° (hot cases) and 310°K (cold cases) and cylinder wall temperatures of 660° and 300°K, respectively. In all cases, the bed pressure was assumed to be atmospheric, the cylinder diameter was 0.0508 m, and the superficial velocity was 1.1 u_{mf}. The lee stack was assumed to extend from a polar angle (θ) of 0.349 rad (20 deg) to 2.79 rad (160 deg) (approximate locations of points of boundary layer separation for flow past a cylinder) and to have a voidage of 0.438. The windward side voidage was assumed to be 0.65, and the ambient voidage was 0.5. For the hot cases, the cylinder wall and bubble boundary emissivities were assumed to be 0.9, and the particle surface emissivity (e_p) was 0.45 (consistent with data given by Baskakov et al. (1973).

The total and convective heat transfer coefficients for the above cases without bubbles present and with and without turbulence ($u' = 0$) are summarized in Table 1. The turbulence intensity used in these calculations is based on data reported by Galloway and Sage (1970). These data as well as those discussed below are generally within the range of experimental results reported by Wright et al. (1970) who obtained a total heat transfer coefficient of about 250 W/m² · °K in a pilot plant coal combustor containing 2.8 mm mean diameter crushed refractory. The effect of turbulence depends upon Reynolds number and is therefore smallest for the lower Reynolds number, high temperature cases as indicated in the table. Also, the contribution of radiation emitted by the hot particles is about 33% of the total heat transfer at combustion conditions.

Figure 12 shows the effect of a single bubble, having a diameter equal to the cylinder diameter, on the convective Nusselt number distribution for the 3 mm hot case and demonstrates the importance of gas velocity in calculating the convective heat transfer (compare with Figure 11). The effect of a single bubble, equal in size to the cylinder, on the total convective Nusselt number is illustrated as a function of bubble location in Figure 13. The large dots represent the bubble center location, and the two numbers are the convective Nusselt numbers relative to the no bubble case for the 3 mm hot and 6 mm cold cases, respectively. These results indicate that a single bubble of this size has a relatively small effect on the total convective heat transfer (the maximum change was about 27% for bubble locations near the cylinder), and this conclusion is relatively insensitive to operating conditions for large particle beds (the data shown in Figure 13 represent a range of Reynolds number of 840 to 6 500).

The Stokes region for the 3 mm hot case spanned a major portion of the cusped channels (see Adams, 1977), so this particle diameter is near the lower limit of validity of the boundary-layer model used to describe the channel flow.

CONCLUSIONS

The results of this analytical study of heat transfer to a horizontal cylinder immersed in a gas fluidized bed have revealed the following:

1. Cold bed/hot bed correlations of heat transfer must not only consider the effects of fluid property differences but also differences in the relative importance of interstitial turbulence.

TABLE 1. TOTAL HEAT TRANSFER FOR 3 AND 6 MM HOT AND COLD PARAMETERS WITHOUT BUBBLES

		Total convective Nusselt No.		Total convective heat transfer (W/m² · °K)		Total heat transfer (W/m² · °K)	
Case	Re_D	$u' = 0.2$	$u' = 0.0$	$u' = 0.2$	$u' = 0.0$	$u' = 0.2$	$u' = 0.0$
3 mm hot	840	132	125	192	182	268	258
3 mm cold	4 300	244	195	130	103	130	103
6 mm hot	1 550	102	85.7	149	125	226	201
6 mm cold	6 500	263	173	139	92.0	139	92.0

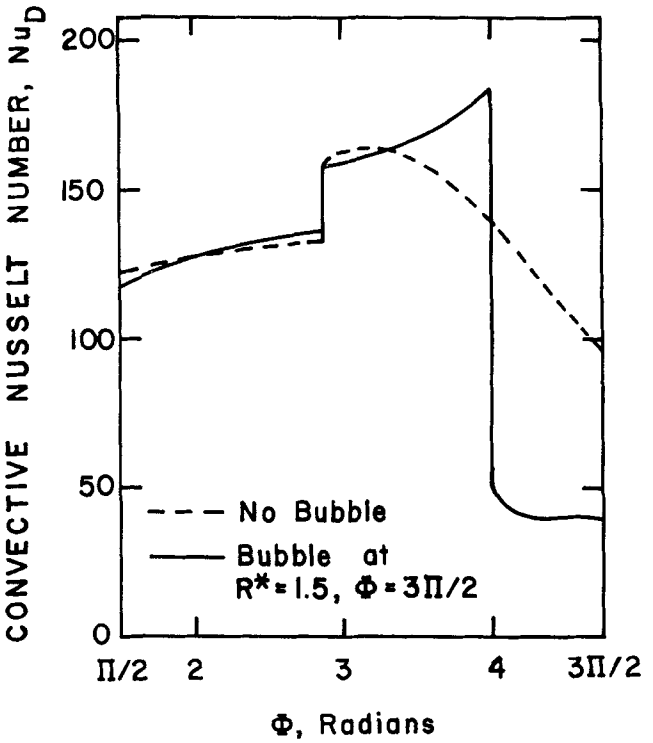

Fig. 12. Convective Nusselt number distribution for 3 mm hot parameters for $R_B^* = 1$.

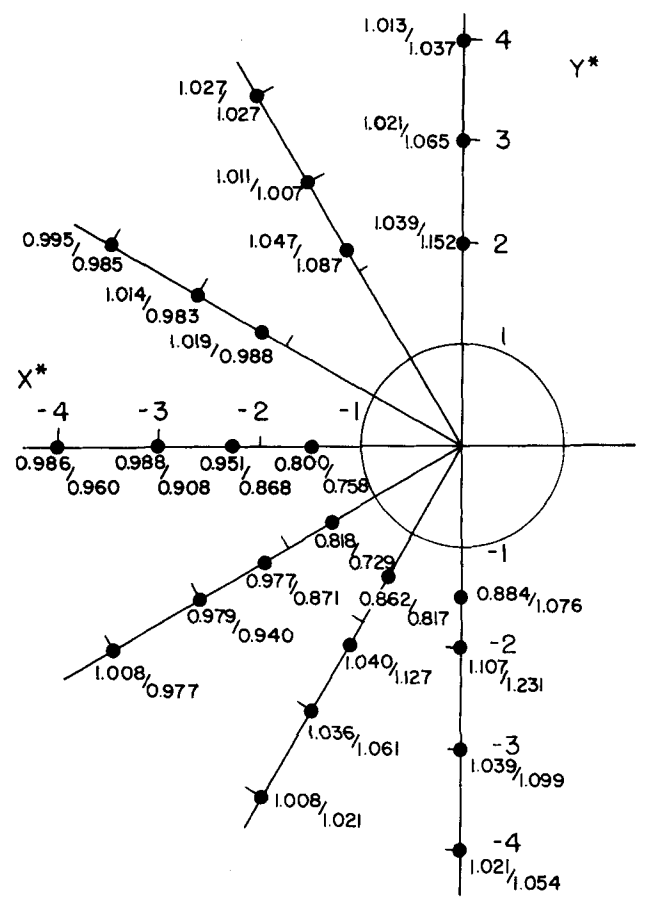

Fig. 13. $(Nu/_D)_{conv}/(Nu_D)_{\substack{conv \\ no\ bubble}}$ for 3 mm hot parameters/6 mm cold parameters with $R_B^* = 1$.

2. The total heat transfer to the cylinder is not strongly affected by the presence of a single two-dimensional bubble having a diameter equal to the cylinder diameter.

3. The total heat transfer coefficients obtained using this gas convection dominant model are within the range of experimental results obtained as a result of controlled hot and cold flow experiments.

4. Gas velocity has a dominant effect on local heat transfer rates, so an important area for further study is more detailed modeling of gas velocity in the vicinity of a horizontal cylinder with bubbles present considering the effects of voidage variations and perhaps three-dimensional bubbles.

5. The assumptions of the model are expected to be valid for particle diameters of 2 to 3 mm and larger.

ACKNOWLEDGMENT

The work reported herein was prepared, in part, for the U.S. Department of Energy under Contract No. EF-77-S-01-2714.

NOTATION

a_1, a_2, a_3, a_4 = velocity profile constants
A_2, A_3 = surface areas in radiative heat transfer analysis
b_1, b_2, b_3, b_4 = temperature profile constants
B_i^R = radiative heat transfer parameter
c_f = skin friction coefficient
c_{f2D} = two-dimensional skin friction coefficient
c_R = Chapman-Rubesin constant,

$$\left(\frac{T_W}{T_B}\right)^{1/2}\left(\frac{T_B + 110°K}{T_W + 110°K}\right)$$

d_p^+ = dimensionless particle diameter, d/D
D = cylinder diameter
e_B = bubble boundary emissivity
e_p = particle boundary emissivity
e_W = cylinder wall emissivity
G_{2H} = thickness ratio, Δ_2/δ_H
h_{max} = maximum heat transfer coefficient for fluidized bed
h_0 = scale factor at $y^+ = 0$
H_{12} = thickness ratio, δ_1/δ_2
H_{2V} = thickness ratio, δ_2/δ_V
i = unit imaginary number, $\sqrt{-1}$
j = summation index
K_g = gas thermal conductivity
K_T = universal constant in turbulence model
K_β = drag coefficient
l_e = turbulence length scale at edge of boundary layer
L = characteristic length
L_c = average particle spacing and length of channel
M = boundary-layer momentum parameter
N = number of bubbles
N_{HV} = boundary-layer thickness ratio, δ_H/δ_V
Nu_D = Nusselt number based on D, $\dfrac{D}{K_g}\dfrac{q_W}{(T_B - T_W)}$
$(Nu_D)_{conv}$ = convective Nusselt number
$(Nu_D)_{\substack{conv \\ no\ bubble}}$ = convective Nusselt number without bubbles
$Nu_{D_1}^R$, $Nu_{D_2}^R$ = effective Nusselt number due to radiation for surfaces (1) and (2), respectively
$(Nu_D)_{\substack{Stokes \\ edge}}$ = Nusselt number at edge of Stokes region
Nu_{D_0} = Nusselt number without turbulence
$(Nu_D)_{2D}$ = two-dimensional Nusselt number
p^+ = dimensionless pressure, $p/\rho u_{mf}^2$
Pr = Prandtl number
q_W = wall heat flux

$\bar{Q}_g^+$ = dimensionless average gas velocity, $\bar{Q}_g/u_{mf}$
$Q_{g\theta}^+$ = tangential gas velocity
r = radial coordinate on circle plane
r_p = particle radius
R^+ = dimensionless radial coordinate, R/D
R_B^+ = dimensionless bubble radius
R_0^+ = radial coordinate of bubble center
R_1 = inner boundary of Stokes region on unit circle
Re_D = Reynolds number based on cylinder diameter, $u_{mf}D/\nu_\infty$
Re_{L_∞} = Reynolds number based on L and u , $u_\infty L/\nu_\infty$
Re_p = Reynolds number based on particle diameter, $u_{mf}d_p/\nu_\infty$
Re_z = Reynolds number based on z, $u_\infty z/\nu_\infty$
$S(0)$ = S at $\theta^+ = 0$, $-C_R/T_B^+ (\frac{1}{2} + T_W^+)$
T_B^+ = dimensionless bed temperature, $T_B/(T_B - T_W)$
$T_{surface}$ = particle surface temperature
T_W^+ = dimensionless wall temperature, $T_W/(T_B - T_W)$
u^+ = dimensionless axial velocity, u/u_{mg}
u_{mf} = minimum fluidizing velocity
u_0 = superficial velocity
u_∞^+ = dimensionless velocity at edge of boundary layer, u_∞/u_{mf}
u' = turbulence intensity, R.M.S. velocity fluctuation/u_∞
v^+ = dimensionless normal velocity, v/u_{mf}
W = boundary layer energy parameter
x_c^+ = corner location
x_s^+ = Stokes region edge location
x^+, y^+ = dimensionless coordinates, $(\ )/D$
z^+ = complex variable, $x^+ + iy^+$
$z_0^+, \bar{z}_0^+$ = bubble center location and complex conjugate

Greek Letters

β_T = relative eddy diffusivity of edge of boundary layer, $\epsilon_{T\infty}/\nu_\infty$
β_1, β_2 = drag parameters
δ = boundary-layer thickness
δ_H = thermal boundary-layer thickness
δ_V = velocity boundary-layer thickness
δ_1 = displacement thickness
δ_2 = momentum thickness
δ_{2D} = two-dimensional boundary-layer thickness
Δ_2 = enthalpy thickness
ϵ = voidage
ϵ_T^+ = dimensionless eddy diffusivity, ϵ_T/ν_∞
ϵ_∞ = ambient voidage
η_H = thermal boundary-layer similarity parameter, ξ/δ_H
η_V = velocity boundary-layer similarity parameter, ξ/δ_V
θ = angular coordinate
θ_0 = angular position of bubble center
θ^+ = dimensionless temperature parameter, $T - T_W/T_B - T_W$
μ_T = temperature profile parameter
ν_∞ = kinematic viscosity at edge of boundary layer
ξ = transformed normal coordinate
ρ = gas density
σ = Stefan-Boltzman constant
Σ = summation
ϕ = angular coordinate on circle plane
ϕ_c = corner location on circle plane, $\phi_0/2$
ϕ_0 = Stokes region extent on circle plane
ϕ_s = particle sphericity
Φ_s = Stokes region matching parameter
Ω_V = velocity profile shape factor

Subscripts

$(\ )_j$ = quantity for j^{th} bubble

Superscripts

$(\ )^+$ = dimensionless quantity
$(\ )^*$ = quantity divided by cylinder radius

LITERATURE CITED

Adams, R. L., "An Analytical Model of Heat Transfer to a Horizontal Cylinder Immersed in a Gas Fluidized Bed," Ph.D. thesis, Oregon State Univ., Corvallis (1977).

Arpaci, V. S., *Conduction Heat Transfer,* Addison-Wesley, Reading, Mass. (1966).

Baskakov, A. P., et al., "Heat Transfer to Objects Immersed in Fluidized Beds," *Powder Technology,* 8, 273-282 (1973).

Baskakov, A. P., and V. M. Suprum, "Determination of the Convective Component of the Heat Transfer Coefficient to a Gas in a Fluidized Bed," *Intern. Chem. Eng.,* **12**, 324-326 (1972).

Basu, P., "Bed to Wall Heat Transfer in a Fluidized Bed Coal Combustor," *AIChE Symposium Series,* No. 176, **74**, 187 (1978).

Batchelor, G. K., *An Introduction to Fluid Dynamics,* Cambridge Univ. Press, England (1967).

Botterill, J. S. M., *Fluid-Bed Heat Transfer,* Academic Press, New York (1975).

———, and A. O. O. Denloye, "Gas Convective Heat Transfer to Packed and Fluidized Beds—1. A Theoretical Model," *AIChE Symposium Series No. 176,* **74**, 194 (1978).

Botterill, J. S. M., and J. R. Williams, "The Mechanism of Heat Transfer to Gas-Fluidized Beds," *Trans. Inst. Chem. Engrs.,* **41**, 217-230 (1963).

Broughton, J., and J. Kubic, "A Model of Heat Transfer in Gas Fluidized Beds," *Intern. J. Heat Mass Transfer,* **18**, 289-299 (1975).

Chung, B. T., et al., "A Model of Heat Transfer in Fluidized Beds," *J. Heat Transfer,* 105-110 (1972).

Gabor, J. D., "Wall-to-Bed Heat Transfer in Fluidized Beds," *AIChE J.,* **18**, 249 (1972).

Galloway, T. R., and H. Sage, "A Model of the Mechanism of Transport in Packed, Distended and Fluidized Beds," *Chem. Eng. Sci.,* **25**, 495-516 (1970).

Kays, W. M., *Convective Heat and Mass Transfer,* McGraw-Hill, New York (1966).

Kunii, D., and O. Levenspiel, *Fluidization Engineering,* Wiley, New York (1962).

Levenspiel, O., and J. S. Walton, "Bed-Wall Heat Transfer in Fluidized Systems," *Chem. Eng. Progr. Symposium Ser. No. 9,* **50**, 1-13 (1954).

Levy, S., "Effect of Large Temperature Changes (Including Viscous Heating) upon Laminar Boundary Layers with Variable Free Stream Velocity," *J. Aero. Sci.,* 459-473 (1954).

Mickley, H. S., and D. F. Fairbanks, "Mechanism of Heat Transfer to Fluidized Beds," *AIChE J.,* **1**, 374-384 (1955).

Rubin, S. G., and B. Grossman, "Viscous Flow Along a Corner: Numerical Integration of the Corner Layer Equations," *Quart. Appl. Math.,* **29**, 169-186 (1971).

Schlichting, H., *Boundary Layer Theory,* 6 ed., McGraw-Hill, New York (1968).

Siegel, R., and J. R. Howell, *Thermal Radiation Heat Transfer,* McGraw-Hill, New York (1972).

Smith, M. C., and A. M. Kuethe, "Effect of Turbulence on Laminar Skin Friction and Heat Transfer," *Phys. Fluids,* **9**, 2337-2344 (1966).

Staub, F. W., "Two-Phase Flow and Heat Transfer in Fluidized Beds," Sixth Quart. Rep., GE Rep. SRD-77-011, Dec, 31, 1976.

Theodorsen, T., and I. E. Garrick, "General Potential Theory of Arbitrary Wing Sections," *NACA Rept. No. 452* (1933).

Traci, R. M., and D. C. Wilcox, "Free Stream Turbulence Effects on Stagnation Point Heat Transfer," *AIAAJ.,* 13, 890-896 (1975).

Wasan, D. T., and M. S. Ahluwalia, "Consecutive Film and Surface Renewal Mechanisms for Heat or Mass Transfer From a Wall," *Chem. Eng. Sci.,* **24**, 1535-1542 (1969).

Wright, S. J., et al., "Heat Transfer in Fluidized Beds of Wide Size Spectrum at Elevated Temperature," *Brit. Chem. Eng.,* **15**, 1551-1554 (1970).

Yoshida, H., et al., "Heat Transfer Between a Wall Surface and a Fluidized Bed," *Intern. J. Heat Mass Transfer*, 12, 529-526 (1969).
Zamir, M., and A. D. Young, "Experimental Investigation of the Boundary Layer in a Streamwise Corner," *Aero. Quart. J.*, 313-339 (1970).
Ziegler, E. N., et al., "Effects of Solid Thermal Properties on Heat Transfer to Gas Fluidized Beds," *Ind. Eng. Chem. Fundamentals*, 3, 324-328 (1964).

Manuscript received July 5, 1978; revision received October 13, and accepted November 13, 1978.

Turbulence Characteristics and Mass Transfer at Air-Water Surfaces

JOHN T. DAVIES
and
FRANCISCO J. LOZANO
Department of Chemical Engineering
University of Birmingham
Birmingham B15 2TT
England

The turbulence intensities and spectra in water very close to an air interface have been measured with a hot wire anemometer. The turbulence in the water has been induced in three ways: with a stirrer, by a submerged jet, and by flow of a thin film of water over inclined plates, both rough and smooth.

We find that the root-mean-square fluctuation velocity $\tilde{v_x}'$ shows for the first system no regular trend with the distance y below the surface, while for the second system $\tilde{v_x}'$ increases markedly as the surface is approached. In water films over the rough plates, $\tilde{v_x}'$ can be as high as four times the shear stress velocity.

The turbulence energy spectra close to the surfaces in the first and second systems show (Figure 6) no extended region of slope $-5/3$, whereas for flow over the plates, there is an appreciable subrange of this slope (Figures 8 and 9).

Intensities of turbulence in the surface region are as high as 30 to 50% in the first system, up to 100% in the second system, and 17% over smooth plates and up to 60% over rough plates.

These turbulence characteristics can be related to the rates of mass transfer for oxygen absorbing into water by comparing plots of $k/D^{1/2}$ with the square roots of the different eddy frequencies. The Levich treatment [interpreted by Equation (15)] gives good agreement with the stirred cell and jet results. For the smooth and rough plates, mass transfer depends on eddies intermediate in size between the x directional and the y directional large eddies. In all cases, the Kolmogoroff eddy frequencies are much too high to correlate with mass transfer rates.

Further, the energy spectra show that 60 to 80% of the total eddy energy lies in the larger eddies, with only 1% (or less) in the Kolmogoroff range.

We conclude that the Prandtl sized eddies, and even larger eddies, determine mass transfer rates at a free surface.

Direct measurement of concentration fluctuation frequencies, using platinum microelectrodes, was found to be unsatisfactory because of the poor frequency response of the amplified signals.

SCOPE

The distribution of the sizes and energies of eddies very close to an air-water surface are measured in different turbulent systems: stirred cells, water jets impinging from below on to a free surface, and thin films of water flowing over smooth and rough plates. The fluctuation velocities, important in mass transfer at free surfaces, were also measured.

The experimental method is to position a hot wire anemometer closely below the free surface. The results were analysed using a Hewlett-Packard correlator.

To determine what sized eddies at a free liquid surface are primarily responsible for mass transfer, the turbulence characteristics are compared with mass transfer coefficients measured for the absorption of oxygen into water.

Previously published theoretical treatments have assumed that either the very large or the very small eddies are dominant in mass transfer at free surfaces. The present work decides this question experimentally.

Correspondence concerning this paper should be sent to John T. Davies. Francisco J. Lozano is with Facultad de Quimica, Universidad Nacional Autonoma de Mexico, Mexico D.F.

0001-1541-79-2309-0405-$01.25.